NANO · MICRO small
www.small-journal.com

Label-Free Optofluidic Nanobiosensor Enables Real-Time Analysis of Single-Cell Cytokine Secretion

*Xiaokang Li, Maria Soler, Crispin Szydzik, Khashayar Khoshmanesh, Julien Schmidt, George Coukos, Arnan Mitchell, and Hatice Altug**

Single-cell analysis of cytokine secretion is essential to understand the heterogeneity of cellular functionalities and develop novel therapies for multiple diseases. Unraveling the dynamic secretion process at single-cell resolution reveals the real-time functional status of individual cells. Fluorescent and colorimetric-based methodologies require tedious molecular labeling that brings inevitable interferences with cell integrity and compromises the temporal resolution. An innovative label-free optofluidic nanoplasmonic biosensor is introduced for single-cell analysis in real time. The nanobiosensor incorporates a novel design of a multifunctional microfluidic system with small volume microchamber and regulation channels for reliable monitoring of cytokine secretion from individual cells for hours. Different interleukin-2 secretion profiles are detected and distinguished from single lymphoma cells. The sensor configuration combined with optical spectroscopic imaging further allows us to determine the spatial single-cell secretion fingerprints in real time. This new biosensor system is anticipated to be a powerful tool to characterize single-cell signaling for basic and clinical research.

1. Introduction

Single-cell analysis is one of the most powerful approaches toward the development of new therapies for serious diseases such as cancer or autoimmune disorders.[1] The recent implementation of advanced analysis technologies (e.g., next-generation sequencing) has boosted our knowledge and understanding of the complex heterogeneity in cellular genomics, epigenomics, and transcriptomics.[2] However, the analysis of individual cell secretion is essential to fully understand the functional heterogeneity and decipher the underlying mechanisms of cellular interactions and communication. Intercellular signaling and formation of cellular networks is a highly dynamic process mediated by the expression and secretion of small proteins (e.g., cytokines) and other molecules, which identify the particular cell activities, behaviors, and functions.[3,4] The sensitive monitoring and analysis of cell secretion provide invaluable information of the specific functionality and real-time activity of individual cells in either physiological or pathological process. Such dynamic and accurate analysis is still an unresolved challenge. Traditional secretion analysis techniques include enzyme-linked immunosorbent assay (ELISA) or immunofluorescence staining; however, these methods lack sufficient sensitivity for detection of single-cell secretions.[5]

The past few years have seen the advances of innovative strategies for both cell isolation and protein secretion analysis to enable single-cell resolution.[6–9] For instance, Love et al. introduced a large-scale microengraved array which is able to generate the populational secretion profiles from single hybridoma cells,[6] or even to characterize the cytokine secretion of single T lymphocytes upon different activation scenarios.[9] While their methods are efficient enough to provide a high-throughput dataset, the intensive washing steps involved in the fluorescence labeling procedure dramatically impairs the temporal resolution (limited to a few hours) of the analysis. On the other hand, droplet microfluidics has been presented as a promising platform for single-cell sorting and analysis.[10–12] The technique basically involves encapsulating individual cells in droplets loaded with specific fluorescent antibodies or enzymes for capturing and detecting the secreted cytokines. However, subsequent cytokine quantification requires external readout means, such as flow cytometry or spectroscopic methods that increase the overall system complexity and only provide an end-point result. Despite the capabilities of these new techniques for single-cell isolation, the need of either fluorescent or enzymatic labels for detection significantly impairs the dynamic analysis and monitoring of the secretion in real time.

X. Li, Dr. M. Soler, Prof. H. Altug
Institute of Bioengineering
École Polytechnique Fédérale de Lausanne (EPFL)
CH-1015 Lausanne, Switzerland
E-mail: hatice.altug@epfl.ch
C. Szydzik, Dr. K. Khoshmanesh, Prof. A. Mitchell
School of Engineering
RMIT University
Melbourne 3001, Australia
Dr. J. Schmidt, Prof. G. Coukos
Ludwig Institute for Cancer Research
University of Lausanne and Department of Oncology
University of Lausanne
CH-1007 Lausanne, Switzerland
The ORCID identification number(s) for the author(s) of this article can be found under https://doi.org/10.1002/smll.201800698.

DOI: 10.1002/smll.201800698

Label-free biosensors emerge as a unique solution for the sensitive, accurate and real-time analysis of cell secretion.[13–15] This detection scheme circumvents the tedious and costly molecular tagging and enables the elucidation of biomolecular interactions in a noninvasive and dynamic manner. Among various label-free sensing platforms, optical biosensors are distinguished by their compatibility with physiological solutions, robust performance, and ability to perform quantitative detection.[16–20] The recent advances in nanotechnology have inspired the development of extraordinarily improved optical biosensors based on photonic nanostructures. Nanophotonics, by supporting strong light-matter interaction and dramatically confining light in small volumes, enables ultralow detection limits, exceptional miniaturization, and ultimate on-chip integration.[21] Particularly, plasmonic nanohole arrays (NHAs) have demonstrated a unique potential and flexibility for the implementation of powerful biosensors with high-throughput analyses and capabilities for point-of-care deployment and utilization.[22,23] Nanohole arrays can be manufactured with cost-efficient and straightforward techniques,[24] and they overcome the primary constraints of conventional surface plasmon resonance (SPR) devices, such as the light coupling requirements and the limited field of view for high-throughput assays.[25] Furthermore, gold NHA biosensors have demonstrated exceptional performance for the analyses of proteins and cells in a real-time and multiplexed label-free configuration.[24,26–28]

However, label-free photonic biosensors face critical challenges for addressing single-cell secretion analysis. Cytokines are relatively small molecules (MW 15–30 kDa) and are secreted in minute amounts (femtograms per cell per day). Therefore, the direct detection of single-cell secretion in real time without any signal amplification is not straightforward. In order to achieve the ultrahigh sensitivity required for the detection of cytokines secreted from an individual cell, it can be effective to minimize the local volume surrounding the cells by encapsulating them with microchambers. This will result in concentrated molecular distribution in the vicinity of the sensor surface. In this regard, microfluidics technology offers a powerful tool to create a highly miniaturized environment with compartmentalization for the analysis.[29] Nevertheless, the optical monitoring of an ultralow volume in cell culture conditions (i.e., 37 °C) introduces a significant evaporation problem. This is especially challenging when using polydimethylsiloxane (PDMS) as the material for microfluidics. This widely used material provides excellent transparency and high gas permeability, making it an ideal substrate for optical cellular bioassays.[30] However, the gas diffusion also leads to evaporation and associated optical noise when handling the ultralow volume of fluid.[31,32] Water evaporation through PDMS membranes may cause not only an increase in osmolality of the cell media but may also result in bubble formation and eventually dehydration of the cell chamber. These evaporation-mediated osmolality alterations induce local changes of the fluid refractive index, causing dramatic optical signal fluctuations that overwhelm the low magnitude secretion signature of single cells. Conventional approaches to prevent liquid evaporation, such as sealing the aqueous surface with mineral oil[31] or placing numerous sacrificial drops in the vicinity of the analyte chamber,[32] can be effective but increase overall system complexity, limit on-chip integration and pose potential contaminations to the assay. Conversely, thin PDMS membranes between culture areas and oxygen equilibrated water channels have been shown to reduce evaporation, while at the same time maintaining oxygen levels required for sustained culture.[33]

In this work, we introduce a new approach for the single-cell secretion analysis in real time using a label-free nanoplasmonic biosensor. We have developed an optofluidic device based on a gold nanohole array sensor integrated into an innovative multifunctional microfluidic system for the dynamic and accurate monitoring of cytokine secretion from individual cells (**Figure 1**a). The nanohole arrays covering the entire sensor surface are manufactured uniformly with low-cost and wafer-scale photolithography. For optical detection, we exploit a spectroscopic imaging method which converts each imaged point to an effective sensing element. We utilize the single step injection molding technique[34] to create a microfluidic system equipped with pneumatic valves that enables both the in-flow introduction of cells into the device and isolation of a microchamber

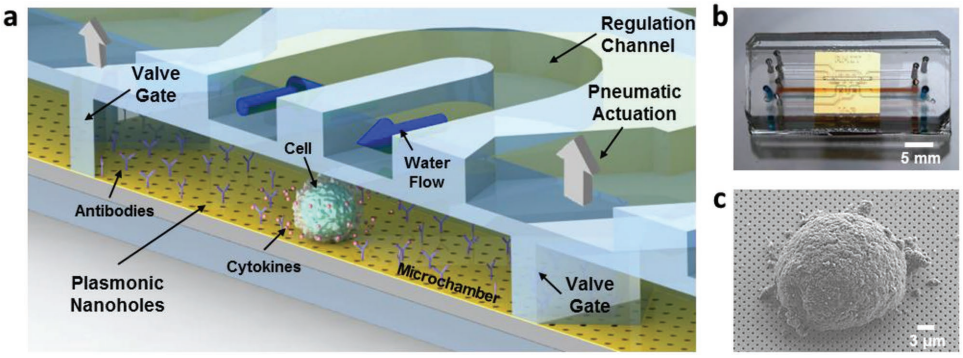

Figure 1. Illustration of the optofluidic system for real-time single cell analysis. a) Schematic representation of the microfluidic-integrated nanoplasmonic biosensor. The microfluidic system consists of two fundamental parts: a primary channel in contact with the plasmonic nanohole array chip, which includes two pneumatic valve gates for enclosing a small-volume microchamber for single-cell analysis, and a hydraulic regulation channel fabricated on top of the microchamber to provide humidity regulation through serpentine water flow. For analysis, the single cells attached to the plasmonic chip surface are surrounded by specific antibodies, which will capture the secreted cytokines postactivation. b) The picture of the integrated device. We highlight the primary channel (orange) and the regulation channel (blue) with flowing colored dyes, respectively. c) An SEM image of a single EL4 cell attached to the nanohole array chip.

on the nanostructured sensor chip to confine and analyze individual cells. A valve-gated microchannel allows us to control the flow when introducing the cells that are then isolated within a low volume cell chamber, which maintains the cytokine concentration at a high level and improves the biodetection accuracy. Moreover, we harness the ability of our injection molding approach to create a continuous regulation channel that interacts with the underlying valve-isolated sub-microliter cell chamber through thin PDMS membranes (Figure 1a). The regulation flow simultaneously ameliorates evaporation, prevents bubble formation and enables a stable optical background signal for robust monitoring of single cell secretion analysis.

Our optofluidic device (Figure 1b) has been applied for the label-free detection of interleukin-2 (IL-2) from individual EL4 lymphoma cells (Figure 1c) in a real-time manner. The secretion dynamics can be monitored for a period spanning several hours, without any need to disturb the cell culture and label the secreted cytokine molecules, while keeping the appropriate temperature and humidity conditions for cell activity and viability. The temporal detection interval can be highly customized to ensure sufficient time resolution for the bioanalysis. Furthermore, due to the extended arrangement of NHAs over the entire chip surface, we have the flexibility to designate multiple detection areas around a single cell with varying distances apart, where the cytokine diffusion activity can be depicted spatially as well. This versatile optofluidic biosensor provides a reliable and facile label-free detection platform to investigate the onset, dynamics, and diffusion of cytokine secretion activities at the single-cell level.

2. Results and Discussions

2.1. Optical Configuration of The NHA Biosensor

The plasmonic nanohole arrays offer highly sensitive label-free biosensing and are distinguished among other state-of-the-art plasmonic sensors due to the well-proven capabilities for device miniaturization, multiplexed analysis, and easy integration in lab-on-a-chip devices.[14,22,27] The current fabrication process for nanoplasmonic sensors requires sophisticated and costly techniques, such as e-beam lithography. This inevitably hinders the implementation of nanoplasmonic technology for routine biological analysis. Therefore, we have employed a nanofabrication procedure[35] enabling efficient and large-scale production of plasmonic NHA chips, which minimizes the costs and promotes the real application both in research and clinical fields. The fabrication process is based on deep-UV photolithography technique (Figure S1, Supporting Information) by using robust quartz wafers as the sensor substrate. As a result, we obtained 4-inch diameter wafers (**Figure 2**a) patterned with

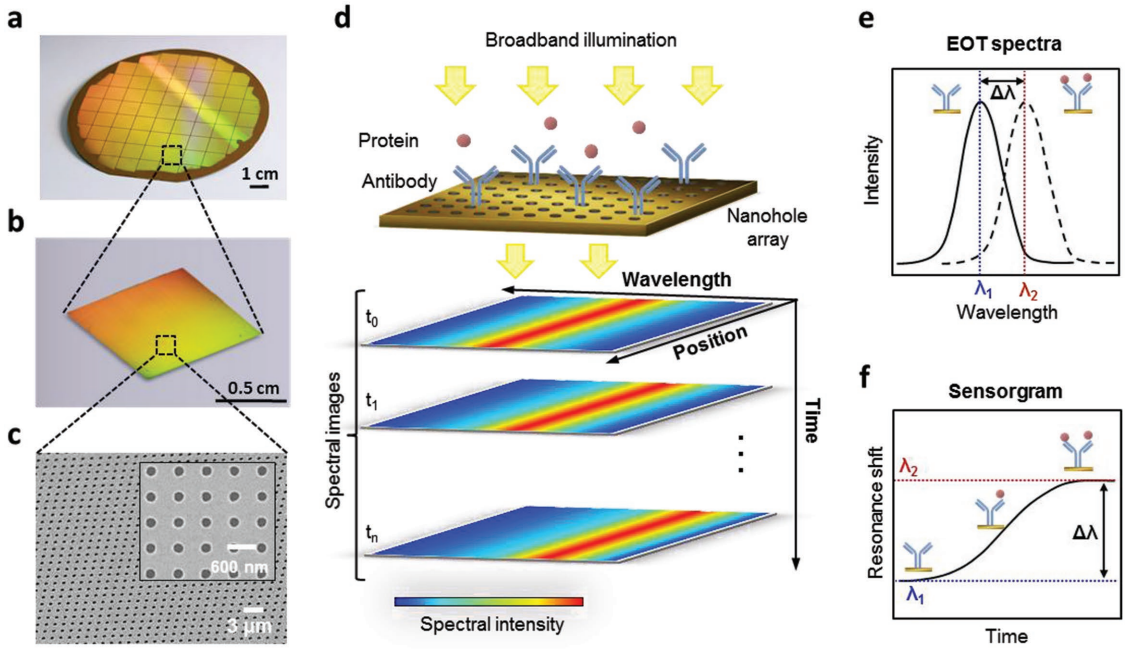

Figure 2. Configuration and working principle of the plasmonic nanohole array biosensor. a) The plasmonic nanohole arrays are fabricated uniformly on a thin gold film by wafer-scale deep-UV photolithography over the entire 4-inch diameter quartz wafer. b) The nanopatterned wafer is diced to 1×1 cm^2 sensor chip for analysis. The appearance of colors on the chip when viewed at a tilt shows the diffraction grating effect resulted from the nanohole arrays on its surface. c) An SEM image shows the uniformly distributed nanohole structures on the quartz substrate, where the nanoholes have a diameter of 200 nm and are separated center-to-center by 600 nm. d) The chip functionalized with biorecognition elements is illuminated normally with a broadband light source, exciting the surface plasmons which can be characterized by the appearance of specific EOT resonance peaks in the transmitted light. The transmission spectra are recorded and analyzed by the spectroscopic imaging setup, forming spectral images over time from t_0 to t_n. The two axes of the spectral images correspond to spatial position and wavelength. Upon analyte binding to the biorecognition elements, the change of refractive index on the plasmonic surface induces a wavelength shift of the resonance peak of the transmitted light. e) The spectral wavelength shift of the EOT resonance peak extracted from the spectroscopic images can be quantified directly in proportion to the changes of refractive index due to accumulated mass on the nanohole array surface. f) A sensorgram is obtained by tracking the resonance shift in real time, enabling the monitoring of biomolecular binding in a label-free manner.

uniform arrays of gold nanoholes (200 nm diameter, 600 nm period) across the entire wafer surface as confirmed by SEM image analysis (Figure 2c). Wafers were further diced into small sensor chips of 1 × 1 cm^2 (Figure 2b) for cell analysis. The working principle of this biosensor is based on the phenomenon of extraordinary optical transmission (EOT), which is represented as a dramatic enhancement of light transmission through the regularly periodic subwavelength nanohole structures.[36,37] This light enhancement is characterized by the appearance of an EOT resonance peak in the transmission spectrum. The EOT resonance is highly sensitive to minute changes in the near-field refractive index over the nanohole surface. The molecular binding on the sensor surface induces a variation of the refractive index that leads to a spectral shift of the peak wavelength (Figure 2d). By tracing the spectral shifts with ongoing experiment time, we are able to depict the molecule binding events in a real-time format.

We characterized the performance and sensitivity of our NHA biosensor for label-free spectroscopic imaging. For the measurements, we placed the sensor chip on an inverted microscope where a collimated broadband light source illuminated the NHAs at normal incidence, resulting in the onset of EOT phenomenon (Figure S2, Supporting Information).[38] The transmitted light was collected by the objective underneath and coupled to a spectrometer through a 500 μm wide slit opening. The spectral content is then dispersed by a grating (600 lines mm^{-1}) and recorded on a 1024 × 1024 pixel CCD camera with a pixel size of 13 × 13 μm^2. The recorded CCD image consists of a spatially resolved 1D spectral image in which the horizontal axis represents the range of optical wavelength while the other represents the positions across the illuminated area of the NHAs through the slit opening (Figure 2d). By adjusting the wavelength to the EOT resonance position (i.e., ≈860 nm in aqueous solution), we can directly observe the EOT peak (Figure 2e) and monitor the spectral displacements in real time (Figure 2f). To evaluate the system sensitivity, we carried out a bulk refractive index calibration, which was determined to be 630 nm RIU^{-1} (Figure S2, Supporting Information). This sensitivity outranges the majority of the state-of-the-art nanoplasmonic biosensors, demonstrating the unique potential of our system to perform single-cell secretion analysis.[21,39,40]

2.2. Surface Functionalization of NHA Biosensor for Cell Capture and Cytokine Detection

The establishment of a robust and stable surface chemistry strategy is critical in affinity-based biosensors to ensure sensitive, selective and reliable biodetection of the analytes-of-interest from a complex matrix such as cell media. This is particularly essential for in situ single-cell analysis since we ought to coimmobilize both cell and cytokine capturing probes (i.e., antibodies) for an extended period of time. **Figure 3**a illustrates the schematics of the designed surface functionalization. First, we coated the gold chip surface with an antifouling self-assembled monolayer (SAM) composed of polyethylene glycol (PEG) derived compounds, preventing binding of nonspecific molecules.[41] In particular, a mixture of two kinds of PEGylated alkanethiols was employed, with one carrying a reactive carboxylic functional group (−COOH) and the other nonreactive hydroxyl group (−OH), respectively. The latter serves as a lateral spacer to minimize steric hindrance effects during protein attachment. The reactive carboxylic groups were subsequently activated by the general carbodiimide chemistry (i.e., EDC/NHS activation) that allows covalent binding of molecules presenting terminal amine groups (−NH2). At this point, we coimmobilized a mixture of streptavidin and poly-L-lysine (PLL), both containing a significant amount of terminal amine groups. PLL is a well-known polymer with the positive net charge that acts as an electrostatic force to attach floating cells (negative net charge),[42] avoiding any chemical modification of the cell membrane and therefore ensuring immobilization without affecting the cell physiology. Streptavidin was in turn used for the highly stable and oriented immobilization of biotinylated antibodies (Ab) against the cytokine of interest (IL-2). We tested the efficacy of our surface chemistry strategy for both cell attachment and cytokine detection, by depositing a cell suspension sample on the functionalized chip and incubating for 1 h at 37 °C. After carefully rinsing, we confirmed the presence of cells immobilized on the NHA surface by scanning electron microscopy (Figure 1c).

To evaluate the biosensor sensitivity for cytokine detection, we performed a calibration curve with standard protein samples. Samples spiked with different concentrations of recombinant IL-2 proteins (from 50–1000 pg mL^{-1}) were introduced over the functionalized NHAs. We employed a conventional PDMS microfluidic system with microchannels (500 μm wide, 180 μm high) for the sample injection, which was connected to a syringe pump for a continuous buffer flow. As shown in Figure 3b, the capturing of IL-2 to the antibodies was depicted by resonance shifting ($\Delta\lambda$) in a concentration-dependent manner. Higher concentrations of IL-2 samples lead to a greater resonance shift, as well as the progression of signals being accelerated with increasing concentrations. The plateau $\Delta\lambda$ values obtained from each sample were then plotted as a function of the corresponding concentrations. By fitting to a nonlinear regression model (Figure 3c), we determined the limit of detection (LOD) of our biosensor, which is defined as the concentration with a signal amplitude corresponding to three times the standard deviation of the blank signal.[43] Based on the background signal we obtained from the zero-spiked sample, we achieved an outstanding LOD of 39 pg mL^{-1} (2.6 pM) for IL-2 detection.

2.3. Design and Characterization of the Multifunctional Microfluidic System

Renewal of continuous media flow as employed in conventional microfluidic cell assays is not practical for single cell analysis, as it inhibits the accumulation of cell secretions, and thus results in depletion of target molecules. Isolating target cells within an enclosed volume, and minimizing this incubation chamber size would naturally facilitate sensitive biodetection required for single-cell resolution, through minimization of diffusive target loss. However, a number of challenges emerge. The intrinsic property of high gas permeability of thin PDMS membranes enables this material to be ideal for live cell culture. However,

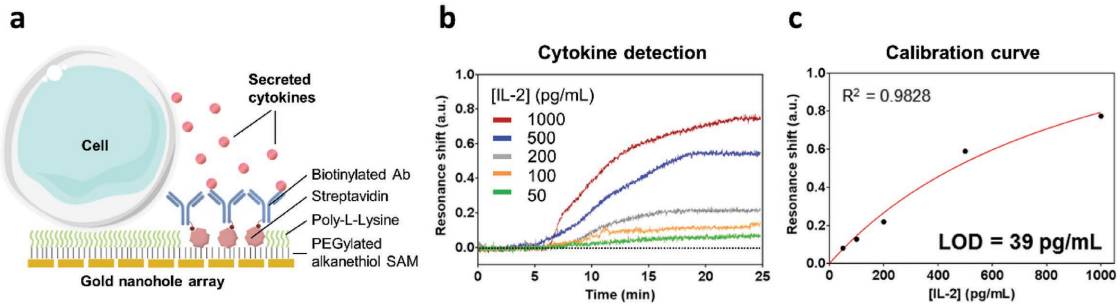

Figure 3. Surface chemistry and characterization of the NHA biosensor for IL-2 detection. a) Surface functionalization strategy for cell attachment and in situ detection of secreted cytokines: the gold surface is modified with a PEGylated alkanethiol self-assembled monolayer (SAM), functional groups of the SAM (COOH) are activated to bind to a mixture of streptavidin and poly-L-lysine covalently. Streptavidin is used to firmly attach the biotinylated antibodies against the target cytokines, while poly-L-lysine to stabilize the anchoring the cells on the sensor surface. b) Real-time sensorgrams of different concentration of cytokines (IL-2) ranging from 50 pg mL^{-1} to 1 ng mL^{-1}. c) Standard calibration curve for direct and label-free detection of IL-2 molecules. Each data point represents the mean value of 3 replicates. The limit of detection (LOD) is determined as the signal corresponding to three times the standard deviation of the blank.

this permeability also leads to evaporation of water through the PDMS structure, which can be problematic for long-term experiments. The significant degree of evaporation and subsequent shift in refractive index hampers the nominal operation of the NHA biosensor (**Figure 4**a).

We experimentally verified the detrimental effects of fluidic evaporation through bulk PDMS on sensor reliability with a basic microfluidic channel design placed within a 37 °C environment (Figure 4b). The evaporation induced significant drift in the resonance response compared to room temperature with the same relative humidity and under the same illumination scheme. Whereas, we obtained a more stable optical readout by supplying doubled humidity surrounding the microfluidics placed in a custom humidity box. This experiment confirmed

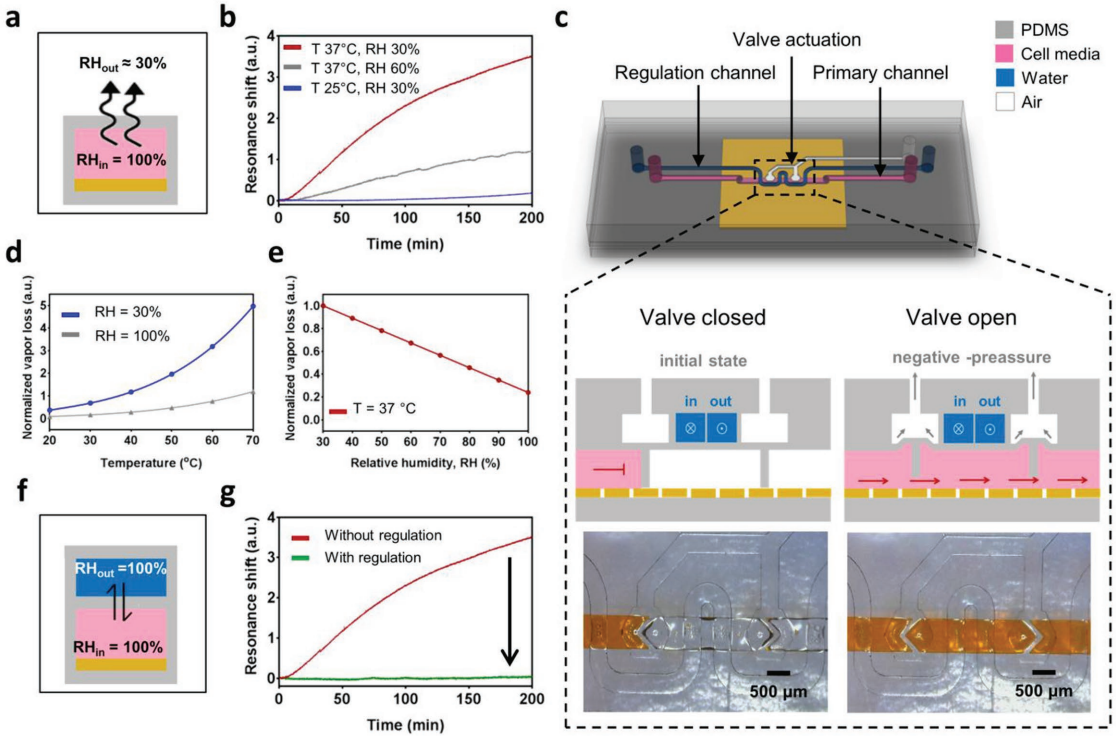

Figure 4. Design and characterization of the microfluidic system. a) Schematic illustration representing the evaporation of water from the PDMS microchamber (RH_{in}) to the surroundings (RH_{out}). b) Baseline drifts of the resonance peak under different conditions surrounding the microchamber with varying temperature and relative humidity. c) Schematic representation of the microfluidic system design with the primary channel for cell injection and culture (pink), pneumatic actuation (white) and the regulation channel blue). Zoom-in figures represent the cross-sectional view of the microfluidic system and the valve actuation mechanism. Real pictures of the microfluidic system are shown at the bottom. d) Numerical calculations of the vapor loss dependency on the temperature at different relative humidity. e) Numerical calculations of the vapor loss dependency on the relative humidity at 37 °C. f) Schematic illustration representing the compensation for the evaporation by the regulation channel filled with water. g) Baseline drift comparison of the sensor signal obtained without regulation (red) and with the regulation system (green) filled with water (100% humidity).

that relatively high humidity is crucial to prevent evaporation and therefore to facilitate stable optical measurements.

In order to stabilize optical response under cell culture conditions, we have designed a novel multilayered microfluidic system utilizing our recently introduced injection molding fabrication technique (Figure S3, Supporting Information).[34] This system allows an isolated microchamber (Length × Width × Height ≈ 2 mm × 500 µm × 180 µm) with a chamber volume of 180 nL for cell measurements while compensating for vapor loss across the gas permeable PDMS structure. The microfluidic device utilises normally closed pneumatically actuated microvalves to isolate the fluid within the small incubation chamber. A schematic of this system is shown in Figure 4c. The primary channel is fabricated in the bottom layer for simple introduction of cells to the biosensor and potential cell retrieval after analysis. The upper layer incorporates the pneumatic lines and actuation chambers required to actuate the isolating microvalves, and a serpentine hydraulic regulation channel to regulate the local humidity and temperature of the incubation chamber. This is facilitated through a thin PDMS membrane present between the regulation and primary channel.

Evaporation of water occurs due to the vapor pressure difference across the wet and dry sides of a PDMS membrane. Based on the theoretical evaluation (Supporting Information 1.3), the evaporation rate through a PDMS membrane would mainly depend on the surface area and thickness of the membrane as well as the temperature and relative humidity of the ambient environment. Using this equation, we calculated the evaporation rate versus different environmental parameters, particularly the typical cell culture temperature (i.e., 37 °C). As shown in Figure 4d, increasing temperature promotes evaporation. In contrast, elevating the relative humidity on the wet membrane minimizes the evaporation from the incubation chamber, and ultimately reduces to nearly zero at a relative humidity of 100% (Figure 4e), which corresponds to the conditions when the regulation channel is filled with water, as shown in Figure 4f. At this point, although the vapor loss through the bulk PDMS and dry membranes persist, it is compensated by vapor transfer across the wet membrane driven by resulting vapor pressure difference. This is evidenced by the improved stability of the signals shown in Figure 4g.

2.4. Real-Time Analysis of IL-2 Secretion from Single EL4 Cells

After characterization and optimization of our optofluidic biosensor, we examined the performance for direct and label-free single cell IL-2 secretion analysis. IL-2 is one of the essential cytokines that are actively involved in numerous biological activities of the immune system, and it particularly exerts prominent functions in regulating the proliferation, activation, and differentiation of T lymphocytes.[44] Therefore, the dynamic analysis of IL-2 secretion events provides insights to better understand its pathophysiological roles in the immune system as well as its potential applications in disease treatments. We selected EL4 lymphoma cells for our experiments, as these cells are engineered to secrete IL-2 cytokines only upon defined chemical stimulus,[45] which represent an optimum IL-2 secretion cell population to evaluate the sensitivity and specificity of our new analytical platform.

To perform the assay, we functionalized the nanoplasmonic chip as described before and assembled it with the multilayer microfluidic system. EL4 cells suspended in cell media were introduced into the primary channel with an ultralow cell density. The pneumatic valves were subsequently closed to stop the flow which resulted in a few isolated single cells being enclosed in the valve-gated chamber (**Figure 5**a). After a short period of incubation at 37 °C to allow firm cell attachment to the NHA surface, the optofluidic device was placed in the inverted microscope equipped with a customized incubator box that provides the proper temperature and CO_2 to maintain appropriate cell

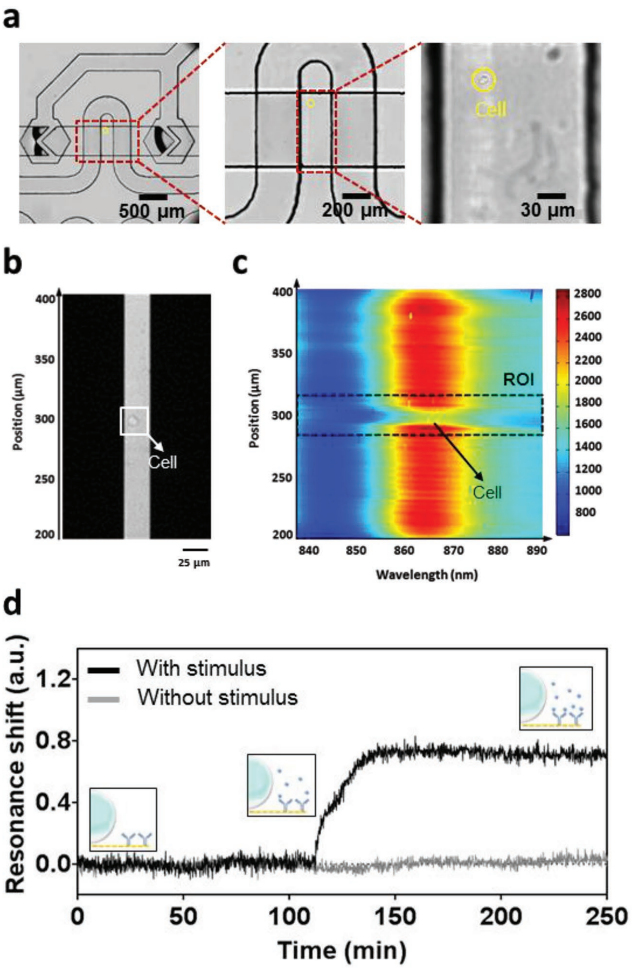

Figure 5. Real-time spectroscopic imaging of single-cell secretion. a) Optical images of an isolated cell encapsulated in the microfluidic chamber. b) CCD image of a single cell positioned in the center of the partially closed slit in the spectrometer. We cropped the image to highlight the attached single cell. Scale bar: 25 µm. c) The 1D spectroscopic image shows the EOT peak intensifies around 865 nm (red region) and the spectral signature generated by the cell spot. The region of interest (ROI, boxed with dashed line) for measurement is defined around the cell spot. d) Real-time sensorgrams obtained from a single EL4 cell secreting IL-2 cytokine upon chemical stimulation (black) and a negative control without the stimulus (gray). Inset figures schematically illustrate the IL-2 secretion and in situ capture by co-immobilized antibodies.

culture conditions. Afterward, a collimated beam of broadband light illuminated the assembled device at normal incidence. We used a 20× magnification objective to image a single EL4 cell. The transmitted light through the NHAs entered the partially open slit in the spectrometer, forming an optical image recorded by the CCD camera as shown in Figure 5b. For illustration purpose, the acquired image was cropped to highlight the location of the cell. By further expanding the recorded image across the wavelength range, we obtained a 1D spectroscopic image (Figure 5c), where the spectral information was revealed alongside the exposed region of the NHAs through the slit. An evident signature in the spectrum appeared at the exact location where the single EL4 cell resides, which resulted from the distinct refractive index of cells. This unique phenomenon allowed us to position a single cell during spectroscopic imaging and define a specific region of interest (ROI) for biodetection. The ROI was subsequently defined in a way that it covers the cell position and the immediate surrounding NHA areas functionalized with anti-IL2 antibodies. In particular, we designated a 40-pixel ROI which corresponds to ≈30 µm on the NHA surface. Then, we extracted the corresponding spectrum of the transmitted light, which shows the EOT resonance peak at ≈860 nm. In order to monitor the capture of analytes in real time, we developed customized MATLAB scripts based on the centroid algorithm[26] to continuously interrogate the resonance peak shifts and to provide a precisely recorded sensorgram. Rather than simply tracking the shifts of maximum peak value, we significantly enhance the signal-to-noise ratio and improve the biosensor sensitivity. We exploited a custom built MATLAB interface that allows ROI definition, spectrum visualizing, centroid calculation and real-time sensorgram display in a user-friendly manner.

To start the analysis, we injected the chemical stimulus including the Ca^{2+} ionophore ionomycin and the phorbol ester PMA into the primary channel to initiate the activation and secretion of the EL4 cell. Immediately following stimulation, we closed the valve gates to keep a static and controlled volume in the cell microchamber. Then, we commenced the continuous monitoring of the peak position that displays the sensorgram in real time (t = 0). As shown in Figure 5d, we observed a significant resonance shift emerging at around t = 110 min (black curve). The signal increase could be directly attributed to the secretion and in situ capture of the IL-2 molecules. We performed an independent negative control experiment employing the same cell culture environment and analysis conditions but without injecting any external stimuli to verify this phenomenon. EL4 cells are a well-characterized cell line that only secretes IL-2 proteins upon proper activation by the chemical stimulus, so cells in common culture media should not produce any sensor response. As can be seen in Figure 5d, the gray line remained stable over the whole analysis duration. The absence of resonance response from the negative control indicates that our biosensor is not only selective for the detection of IL-2 but also repellent to other matrix proteins present in the culture media, avoiding any interference with the cell analysis. We demonstrated that our innovative lab-on-a-chip system is able to detect protein secretion from a single cell in a precise and accurate manner.

2.5. Temporal and Spatial Diffusion Analysis of Single-Cell Secretion

To account for the detection flexibility of our NHA sensing surface, we further exploited the biosensor to characterize the spatial features of single cell secretion in real time. The design of our nanoplasmonic surface with a uniform surface-spanning NHAs enables the simultaneous and independent monitoring of different ROIs. This feature permits not only analysis and detection of single-cell secretion in real time, but observation of the molecular diffusion along the sensor surface. Following the same procedure described before, we introduced different EL4 cells in the biosensor and enclosed them in the microfluidic chamber. **Figure 6**a shows the spectral signature of an isolated cell attached to the NHA chip, and enclosed within the valve-gated PDMS microchamber. In order to analyze the spatial diffusion of the secreted cytokines, we defined different ROIs covering the specific cell spot and surrounding areas (Figure 6b). In this case, each ROI measures 20 pixels in width and separates 40 pixels (center-to-center) away from each counterpart. Considering the overall optical magnification of the system, each ROI was ≈13 µm in width and ≈27 µm in period. The ROIs were extracted as independent spectral curves, and the peak centroids were interrogated in real time (Figure 6c).

We performed this measurement for three independent single EL4 cells (Figure 6d–f). In all cases, we observed a burst of IL-2 secretion at around 110–120 min poststimulation from the cell spot, as well as from the adjacent ROIs (ROI 1 and 1'). There was roughly 20 min of delay for the onset of resonance response from ROI 2/2'. The amount of resonance shifts declined from the cell spot outward, which we attribute to the diffusion process of cytokines in the static media environment. By plotting the endpoint secretion amount of IL-2 (in this case, at 180 min) as a function of different ROIs' locations, we obtained a bell-shaped secretion distribution (Figure 6g–i), where the secretion apex occurred within the central cell spot and declined almost symmetrically outward. It should be mentioned that the label-free biosensing configuration is not able to provide a 3D mapping of the cytokine secretion around the cell, but only the spatial distribution along the sensor surface surrounding the cell. However, the absence of flow in the microchamber and the long-time monitoring might facilitate the secreted cytokines to diffuse effectively across the sensor surface and therefore enable the quantification. The local IL-2 concentration was calculated by interpolating the relative resonance shift to the calibration curve (Figure 3c). We found significant differences among the three different cells. Especially the second measurement (Cell 2) showed a higher amount of secreted IL-2 (2500 pg mL^{-1}) while Cell 1 and Cell 3 appear to secrete less cytokine. This was also reflected in the spatial diffusion analysis, where we observed a more centralized spatial distribution for Cell 2. This phenomenon reveals the intrinsic heterogeneity in a bulk cell population. Whereas by using conventional methods for cell secretion analysis (e.g., ELISA), we would only obtain a single average value for IL-2 secretion at discrete time points. Our single-cell analysis method is promising for accurate observation and precise measurement of protein secretion from individual cells.

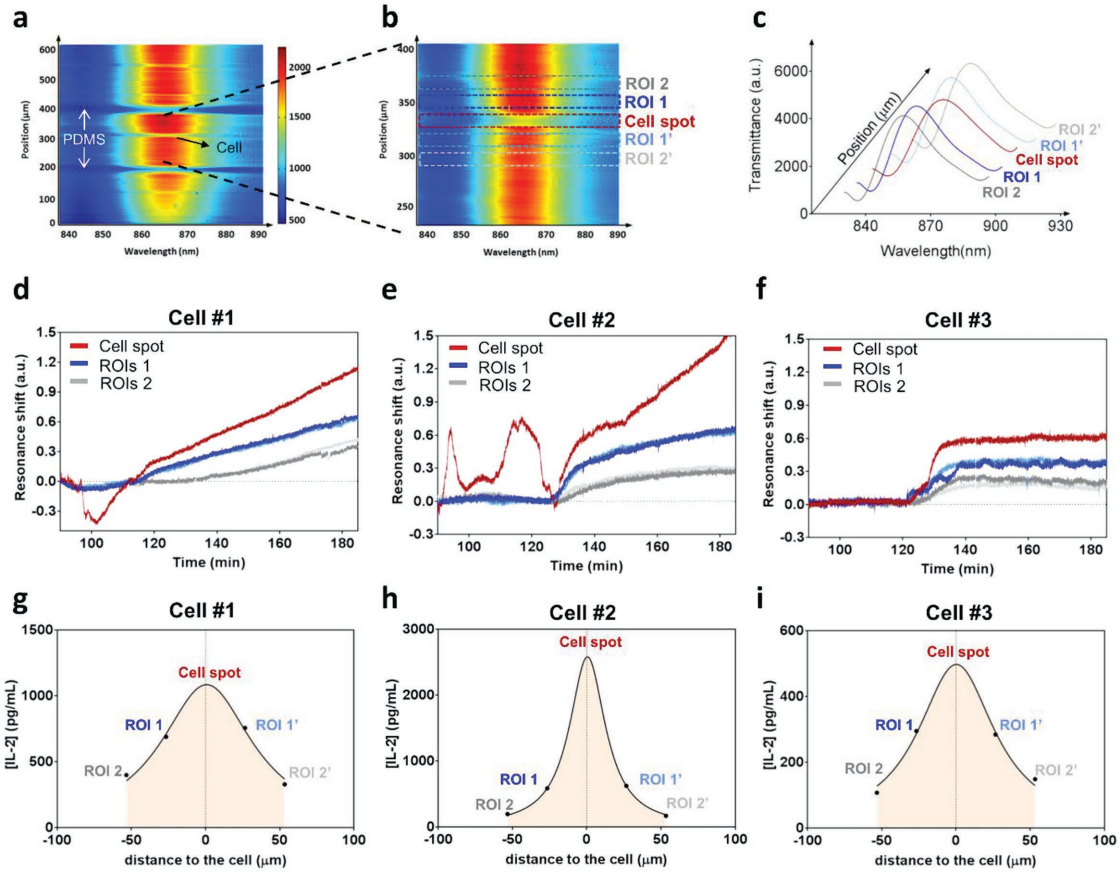

Figure 6. Temporal and spatial diffusion analysis of single cells by label-free spectroscopic imaging. a) Spectral CCD image of the optofluidic system with three isolated cells encapsulated in the microchamber. Strong spectral gaps correspond to the interfacing PDMS of the regulation channel. b) Zoom-in of the spectral image for the ROIs definition at the center cell spot and surrounding areas. c) Spectral EOT peaks corresponding to the selected multiple ROIs. The peaks are interrogated simultaneously and independently. d–f) Independent measurements of IL-2 secretion from three different EL4 cells, monitoring the cell spot ROI and surrounding ROIs simultaneously. g–i) Spatial diffusion analysis of the secreted cytokines: plots correspond to the interpolated concentration of signals acquired for every ROI, fitted to a Gaussian distribution.

It is worth emphasizing that some stochastic noise was observed at the cell spots for Cell 1 and Cell 2 while leaving other ROIs clear of such interference (Figure 6d,e). We could attribute this noise to either cell membrane changes or stochastic cellular movement.[46] In order to prove this hypothesis, we performed another experiment where we split the transmitted light beam to simultaneously image the cell with a CCD camera and measure the plasmonic response. We observed the cell movement within an extremely narrow margin (less than 10 μm) before the onset of cytokine secretion (Figure S4, Supporting Information). This confirms that during the early stage of cell activation, cells undergo certain movements and possible membrane activities. The narrow scope of activity does not influence the detection of cytokines in the surrounding areas. It is important to mention that such phenomena were absent for Cell 3 measurement, while this cell secreted a much lower quantity of cytokines compared to the others. Therefore, the active cell movements could be associated with a higher secretion capacity. Overall, we have demonstrated the superior capabilities of our innovative optofluidic system for the single-cell analysis. This microfluidic-integrated nanoplasmonic biosensor enables a complete analysis of cell activation and secretion from isolated individual cells in a label-free, real-time, and user-friendly manner. By expanding the real-time single-cell analysis to a high-throughput configuration with the incorporation of microfluidic cell traps or other strategies,[47] we would be able to identify and study cell activation and secretion more efficiently. Besides, the possibility of retrieving the cells after the analysis would make our optofluidic sensor an ideal system for its application in biomedical research.

3. Conclusion

We introduce a novel design of an optofluidic nanoplasmonic biosensor for single-cell cytokine secretion analysis. This biosensor platform builds upon the ultrasensitive gold nanohole arrays integrated with an easy to fabricate but sophisticated microfluidic system, enabling real-time monitoring of protein secretion from live cultured cells at single-cell resolution in a label-free manner. The integration of pneumatically actuated valve gates in the microfluidic device generates an isolated chamber with a few nanoliters volume for sensitive cell analysis. In particular, we incorporate for the first time a novel

multifunctional microfluidic design involving both regulation and primary microchannels to tackle the common PDMS-mediated evaporation challenge for reliable biodetection. This novel design circumvents the need for conventional oil sealing or providing a rather high ambient relative humidity, achieving a user-friendly and facile biodetection configuration. With this biosensor setup, we achieved an outstanding sensitivity of 39 pg mL^{-1} for direct IL-2 detection in complex media. The IL-2 molecules secreted from individual EL4 lymphoma cells can also be directly monitored over several hours without interrupting the cell culture. The uniform arrangement of NHAs over the whole sensor chip surface also allows us to elucidate the spatial distribution of cell secretion. Furthermore, the analysis with different single EL4 cells reveals distinct fingerprints for secretion capacity despite their similar phenotypes. With these capabilities, the proposed nanoplasmonic biosensor system represents a powerful tool to analyze cytokine secretion at the single-cell level in a label-free and real-time manner.

4. Experimental Section

Fabrication of NHA-Based Biosensor: The gold NHA chips were manufactured by using wafer-scale and high-throughput nanofabrication techniques on a robust, transparent quartz substrate in a single lithography step. Briefly, Radio Corporation of America (RCA) cleaned 4 inch fused silica wafers were first coated with Ti/Au (10/120 nm) by an e-beam evaporator (Alliance-Concept EVA 760). The Ti layer enabled the Au adhesion on the glass substrate, as well as suppressed the irrelevant surface modes induced by the Au/glass interface. Therefore, only the (1, 0) Au/Medium EOT peak could be monitored through a wide spectral interval, which was critical for wide dynamic sensing range. Next, the NHAs (200 nm diameter and 600 nm period) were patterned using a 248 nm deep-UV stepper (ASML PAS 5500/300 DUV) and were transferred into the Ti/Au layer using an ion beam etching tool (Oxford Instruments PlasmaLab 300 IBE) after developing the photoresist. The resist residuals on the surface were removed by oxygen plasma cleaning. Finally, the 4 inch processed wafer was diced into 1 cm × 1 cm chips for the subsequent optical measurements.

Fabrication of Microfluidic System: Microfluidic devices were manufactured with polydimethylsiloxane (PDMS, SYLGARD 184 SILICONE ELASTOMER KIT) by using a combination of the membrane sandwich fabrication method[48] and PDMS injection molding technique.[34] Figure S3 (Supporting Information) illustrates a pair of complementary molds that were utilized for the injection molding process. Molds were fabricated by standard photolithography techniques,[49] as described in the previous work.[34] In brief, SU-8 3050 (MicroChem Corp) was used to pattern the transparent upper borosilicate glass wafer substrate, and lower silicon wafer substrate with protruding features, with a height of 160 and 180 µm, respectively. PDMS prepolymer was prepared by mixing the silicone elastomer and the curing agent with a weight ratio of 10:1 respectively, followed by thorough degassing in a vacuum desiccator. The prepolymer was introduced between the molds, which were optically aligned and clamped in position under a dissecting microscope. Standoff distance between the molds could be adjusted by changing the spacer material positioned between supporting pillars regularly positioned across the molds. The clamped mold assembly was cured in an oven at 80 °C for 1 h and separated to extract the cured PDMS slab, which was further cut to size and biopsy punched with viaducts providing a pathway between the primary channel and primary channel interface lines. The upper surface was plasma bonded (Harrick Plasma PDC-002: 100% O_2, 1 min) to a 5 mm thick blank PDMS interface slab that was previously biopsy punched with 1 mm interface holes aligning with the interface areas on the fluidic inlets, outlets, and pneumatic interface areas. Microchannels were patterned on both sides of the injection molded slab, namely, the primary channel measuring 500 µm in width for cell culture on the bottom surface, which corresponds to 500 µm wide fluidic interface lines on the upper surface, pneumatic actuation channels and 300 µm wide fluidic regulation channels were also patterned on the upper layer. The fluidic interface lines connected through biopsy-punched viaducts to the accessible interface areas, allowing fluidic access to the primary channel on the bottom layer. The complementary molds were separated by ≈60 µm during PDMS casting, resulting in a thin PDMS membrane (i.e., the regulation membrane) between the regulation and the primary channels. The detailed fabrication process of the pneumatically controlled valves was described elsewhere in a previous work outlining the simplified method by injection molding.[34] In Brief, the valve gates consisted of protruding barriers obstructing fluid flow positioned within the primary channel, directly under the actuation chambers, and forming an isolated channel segment as the incubation chamber. A thin PDMS membrane separated the hexagonal pneumatic actuation chambers and primary channel. When the actuation chambers were evacuated, the valve membranes were deflected upward, raising the valve gates clear of the primary channel floor and allowing fluid flow across the valves. The regulation channel passed in parallel above the primary channel and followed a serpentine configuration directly over the valve-gated area, readily maintaining the steady state of the isolated volume underneath the membrane.

Functionalization and Characterization of the Biosensor for IL-2 Detection: The nanoplasmonic chip was cleaned by consecutive washes in acetone, ethanol, and Milli-Q water, and then further treated with a UV-ozone cleaner (Bioforce Nanosciences) for 20 min. The detailed functionalization procedure is described in our previous publication.[25] Briefly, the cleaned chip was first coated with a mixture of PEGylated alkanethiols in absolute ethanol overnight at room temperature. The carboxylic groups on the chip surface were then activated by incubating with a cross-linking solution containing 200 × 10^{-3} M EDC and 50 × 10^{-3} M sulfo-NHS in 0.1 M MES buffer (pH = 4.5) for 15 min at room temperature. Subsequently, the activated chip was incubated with 0.01% poly-L-lysine and 100 µg mL^{-1} streptavidin solution diluted in phosphate-buffered saline (PBS) overnight at 4 °C, followed by incubation with biotinylated IL-2 antibodies (50 µg mL^{-1}) at room temperature for 1 h.

To determine the bulk refractive index sensitivity, a serial sequence of incrementally increasing dilutions of glycerol solutions with known refractive indices (RI)[50] was introduced in the biosensor and tracked the induced the resonance shifts (Figure S2, Supporting Information). By plotting the resulting wavelength changes ($\Delta\lambda$) and fitting to a linear regression equation, the bulk sensitivity of the sensor (i.e., slope) was determined to be 630 nm RIU^{-1} (Figure S2, Supporting Information).

To calibrate the optical responses to multiple concentrations of IL-2, the standard recombinant IL-2 proteins diluted in PBS with gradient concentrations were injected over the biosensor chip at a flow rate of 20 µL min^{-1}. We utilized a conventional microfluidic system with microchannels (500 µm wide, 180 µm high) for the sample injection, which was connected to a syringe pump for continuous buffer flow. Each concentration was measured in triplicate. The chip surface could be regenerated by injecting 20 × 10^{-3} M NaOH solution post each injection. In addition, the calibration curve does not differ significantly from different dilution medium (i.e., cell medium vs PBS), which excludes possible matrix interferences. The limit of detection (LOD) of the biosensor was defined as LOD = 3 × σ_x, where σ_x is the standard deviation of the background optical signal.

Optical Measurement Setup and Data Processing: A spectrometer (Shamrock 303i, Andor, spectral resolution 0.1 nm) and a deep-cooled CCD camera (iKon-M, Andor) were installed onto an inverted microscope (Nikon Ti-U) to perform EOT-based optical measurements. A broadband tungsten–halogen lamp illuminated the nanoplasmonic chip at normal incidence. For single cell monitoring, the EOT signals were collected using a 20 × objective (CFI Plan Fluor DLL, NA = 0.5) lens from one individual EL4 cell and entered the spectrometer through a 400 µm wide slit opening, forming a 1D spectroscopic image. Andor Solis software was employed to analyze the spectra. Due to the spatial coverage of the

nanostructures over the entire sensor surface, it was flexible to define the measurement loci according to specific needs, namely by selecting different positions of the region-of-interest (ROI). The spectroscopic images were obtained with 0.5 s exposure, and a grating of 600 lines mm^{-1} was used to have sufficient spectral resolution. The spectra were extracted from each ROI on the image by a custom MATLAB image processing script. The resonance peak position was defined by calculating the centroid of the peak within a fixed wavelength window (40% maximum intensity) and plotted in real time. Sensorgrams showed the centroid shifting versus time of multiple ROIs simultaneously. To extract reliable information from cell secretion, the sensorgrams were further normalized employing a control ROI placed on a cell-free region. To quantify the spectral shift and interpolate the calibration curve, curve fitting of the sensorgrams was performed with nonlinear regression using GraphPad Prism 7. The correlation between cytokine diffusion and multiple ROI locations was analyzed by Gaussian Lorentizian distribution.

Supporting Information

Supporting Information is available from the Wiley Online Library or from the author.

Acknowledgements

X.L. and M.S. contributed equally to this work. The authors acknowledge the École Polytechnique Fédérale de Lausanne, Biltema Foundation, ISREC Foundation and Ludwig Institute for Cancer Research for the financial support. The authors thank the Biological Electron Microscopy facility and Center of MicroNano Technology at EPFL, and the MicroNano Research Facility at RMIT for their contribution in SEM imaging and micro-/nano-fabrication.

Conflict of Interest

The authors declare no conflict of interest.

Keywords

cytokine detection, label-free biosensors, microfluidics, nanoplasmonics, real-time single-cell analysis

Received: February 20, 2018
Revised: April 6, 2018
Published online:

[1] J. R. Heath, A. Ribas, P. S. Mischel, *Nat. Rev. Drug Discovery* **2016**, *15*, 204.
[2] D. Wang, S. Bodovitz, *Trends Biotechnol.* **2010**, *28*, 281.
[3] A. Koseska, P. I. Bastiaens, *EMBO J.* **2017**, *36*, 568.
[4] G. C. Tsokos, N. R. Rose, *Clin. Immunol.* **2017**, *181*, 1.
[5] G.-C. Yuan, L. Cai, M. Elowitz, T. Enver, G. Fan, G. Guo, R. Irizarry, P. Kharchenko, J. Kim, S. Orkin, J. Quackenbush, A. Saadatpour, T. Schroeder, R. Shivdasani, I. Tirosh, *Genome Biol.* **2017**, *18*, 84.
[6] J. C. Love, J. L. Ronan, G. M. Grotenbreg, A. G. van der Veen, H. L. Ploegh, *Nat. Biotechnol.* **2006**, *24*, 703.
[7] Y. Shirasaki, M. Yamagishi, N. Suzuki, K. Izawa, A. Nakahara, J. Mizuno, S. Shoji, T. Heike, Y. Harada, R. Nishikomori, O. Ohara, *Sci. Rep.* **2014**, *4*, srep04736.
[8] A. J. Torres, A. S. Hill, J. C. Love, *Anal. Chem.* **2014**, *86*, 11562.
[9] A. J. Torres, R. L. Contento, S. Gordo, K. W. Wucherpfennig, J. C. Love, *Lab Chip* **2013**, *13*, 90.
[10] V. Chokkalingam, J. Tel, F. Wimmers, X. Liu, S. Semenov, J. Thiele, C. G. Figdor, W. T. S. Huck, *Lab Chip* **2013**, *13*, 4740.
[11] Y. F. S. Seah, H. Hu, C. A. Merten, *Mol. Aspects Med.* **2018**, *59*, 47.
[12] Y. Lu, L. Yang, W. Wei, Q. Shi, *Lab Chip* **2017**, *17*, 1250.
[13] S. Sang, Y. Wang, Q. Feng, Y. Wei, J. Ji, W. Zhang, *Crit. Rev. Biotechnol.* **2016**, *36*, 465.
[14] H. Im, H. Shao, Y. I. Park, V. M. Peterson, C. M. Castro, R. Weissleder, H. Lee, *Nat. Biotechnol.* **2014**, *32*, 490.
[15] S.-H. Wu, K.-L. Lee, A. Chiou, X. Cheng, P.-K. Wei, *Small* **2013**, *9*, 3532.
[16] B.-R. Oh, N.-T. Huang, W. Chen, J. H. Seo, P. Chen, T. T. Cornell, T. P. Shanley, J. Fu, K. Kurabayashi, *ACS Nano* **2014**, *8*, 2667.
[17] M. C. Estevez, M. Alvarez, L. M. Lechuga, *Laser Photonics Rev.* **2012**, *6*, 463.
[18] X. Fan, I. M. White, S. I. Shopova, H. Zhu, J. D. Suter, Y. Sun, *Anal. Chim. Acta* **2008**, *620*, 8.
[19] A. B. González-Guerrero, S. Dante, D. Duval, J. Osmond, L. M. Lechuga, *Procedia Eng.* **2011**, *25*, 71.
[20] L. Tu, X. Li, S. Bian, Y. Yu, J. Li, L. Huang, P. Liu, Q. Wu, W. Wang, *Sci. Rep.* **2017**, *7*, 11020.
[21] G. A. Lopez, M.-C. Estevez, M. Soler, L. M. Lechuga, *Nanophotonics* **2017**, *6*, 123.
[22] A. E. Cetin, A. F. Coskun, B. C. Galarreta, M. Huang, D. Herman, A. Ozcan, H. Altug, *Light: Sci. Appl.* **2014**, *3*, e122.
[23] T.-Y. Chang, M. Huang, A. A. Yanik, H.-Y. Tsai, P. Shi, S. Aksu, M. F. Yanik, H. Altug, *Lab Chip* **2011**, *11*, 3596.
[24] C. Escobedo, *Lab Chip* **2013**, *13*, 2445.
[25] D. R. Shankaran, K. V. Gobi, N. Miura, *Sens. Actuators, B* **2007**, *121*, 158.
[26] X. Li, M. Soler, C. I. Özdemir, A. Belushkin, F. Yesilköy, H. Altug, *Lab Chip* **2017**, *17*, 2208.
[27] M. Soler, A. Belushkin, A. Cavallini, C. Kebbi-Beghdadi, G. Greub, H. Altug, *Biosens. Bioelectron.* **2017**, *94*, 560.
[28] J. Park, H. Im, S. Hong, C. M. Castro, R. Weissleder, H. Lee, *ACS Photonics* **2018**, *5*, 487.
[29] J. He, A. T. Brimmo, M. A. Qasaimeh, P. Chen, W. Chen, *Small Methods* **2017**, *1*, 1700192.
[30] S. Halldorsson, E. Lucumi, R. Gómez-Sjöberg, R. M. T. Fleming, *Biosens. Bioelectron.* **2015**, *63*, 218.
[31] Y. S. Heo, L. M. Cabrera, J. W. Song, N. Futai, Y.-C. Tung, G. D. Smith, S. Takayama, *Anal. Chem.* **2007**, *79*, 1126.
[32] E. Berthier, J. Warrick, H. Yu, D. J. Beebe, *Lab Chip* **2008**, *8*, 852.
[33] P. C. Thomas, S. R. Raghavan, S. P. Forry, *Anal. Chem.* **2011**, *83*, 8821.
[34] C. Szydzik, B. Niego, G. Dalzell, M. Knoerzer, F. Ball, W. S. Nesbitt, R. L. Medcalf, K. Khoshmanesh, A. Mitchell, *RSC Adv.* **2016**, *6*, 87988.
[35] F. Yesilkoy, R. A. Terborg, J. Pello, A. A. Belushkin, Y. Jahani, V. Pruneri, H. Altug, *Light: Sci. Appl.* **2018**, *7*, 17152.
[36] L. Martín-Moreno, F. J. García-Vidal, H. J. Lezec, K. M. Pellerin, T. Thio, J. B. Pendry, T. W. Ebbesen, *Phys. Rev. Lett.* **2001**, *86*, 1114.
[37] S. G. Rodrigo, L. Martín-Moreno, A. Y. Nikitin, A. V. Kats, I. S. Spevak, F. J. García-Vidal, *Opt. Lett.* **2009**, *34*, 4.
[38] S. Hoon Lee, N. C. Lindquist, N. J. Wittenberg, L. R. Jordan, S.-H. Oh, *Lab Chip* **2012**, *12*, 3882.
[39] L. Feuz, M. P. Jonsson, F. Höök, *Nano Lett.* **2012**, *12*, 873.
[40] M. Bahramipanah, S. Dutta-Gupta, B. Abasahl, O. J. F. Martin, *ACS Nano* **2015**, *9*, 7621.
[41] T. McPherson, A. Kidane, I. Szleifer, K. Park, *Langmuir* **1998**, *14*, 176.

[42] D. Mazia, G. Schatten, W. Sale, *J. Cell Biol.* **1975**, *66*, 198.
[43] ACS Committee on Environmental Improvement, *Anal. Chem.* **1980**, *52*, 2242.
[44] S. L. Gaffen, K. D. Liu, *Cytokine* **2004**, *28*, 109.
[45] J. J. Farrar, J. Fuller-Farrar, P. L. Simon, M. L. Hilfiker, B. M. Stadler, W. L. Farrar, *J. Immunol.* **1980**, *125*, 2555.
[46] M. P. Raphael, J. A. Christodoulides, J. B. Delehanty, J. P. Long, J. M. Byers, *Biophys. J.* **2013**, *105*, 602.
[47] T. W. Murphy, Q. Zhang, L. B. Naler, S. Ma, C. Lu, *Analyst* **2018**, *143*, 60.
[48] J. R. Anderson, D. T. Chiu, R. J. Jackman, O. Cherniavskaya, J. C. McDonald, H. Wu, S. H. Whitesides, G. M. Whitesides, *Anal. Chem.* **2000**, *72*, 3158.
[49] H. Lee, K. Lee, B. Ahn, J. Xu, L. Xu, K. W. Oh, *J. Micromech. Microeng.* **2011**, *21*, 125006.
[50] L. F. Hoyt, *Ind. Eng. Chem.* **1934**, *26*, 329.